

Wide-band Beamformer with Integrated Antennas

AMIRHOSSEIN FEREIDOUNTABAR
Telecommunication Company of Isfahan
University of Applied Sciences and Technology
Tehran
IRAN
amir_h_f_t@yahoo.com

Abstract:

As part of the development of a new international radio-telescope SKA (Square Kilometer Array), three phased-array prototypes with increasing complexity have been developed. The final SKA telescope will consist of more than one million receiving antenna elements and will operate in the frequency range of 200 to 2000 MHz. One of the challenges of the next generation radio telescopes for astronomy is its capacity to cope with the increasing problem of Radio Frequency Interference (RFI). The application of phased-array beamforming techniques opens the possibility to spatially null RFI in the digital domain prior to correlation. This paper presents results from the third phased-array experimental demonstrator that is being developed at NFRA, the THousand Element Array (THEA), on the RF Beamformer boards with integrated antenna array.

Keywords: Beamforming, Antenna arrays, Wideband beamformer, Sensitivity, Integrated antennas, Dual beam, Measurement, Testing

1 Introduction

The next generation of radio telescopes will be two orders of magnitude more sensitive than telescopes currently in use. A strawman design of this new telescope, the Square Kilometer Array (SKA), was defined by the international radio-astronomy community [1], [2]. A scientific case has been formulated for the development of this radio telescope in the frequency range of 200 to 2000 MHz with sub-microJansky sensitivity. The specified sensitivity then determines that the telescope should have a total collecting aperture of approximately one square kilometer. One of the options for the new radio telescope is to use a phased array consisting of more than one hundred million receiving antenna elements. Phased arrays offer the unique capability to suppress unwanted RFI signals effectively. In addition, multiple beams can be formed simultaneously with no loss in sensitivity. In 1995, NFRA started with a R&D program that should finally lead to the SKA telescope. In the first stage of this R&D program

three phased-array demonstrators with increasing size and complexity are being developed and tested. The One Square Meter Array (OSMA) is the second experimental demonstrator that was developed and tested with 64 active antenna elements [3]. Currently, a third demonstrator is developed, the Thousand Element Array (THEA).

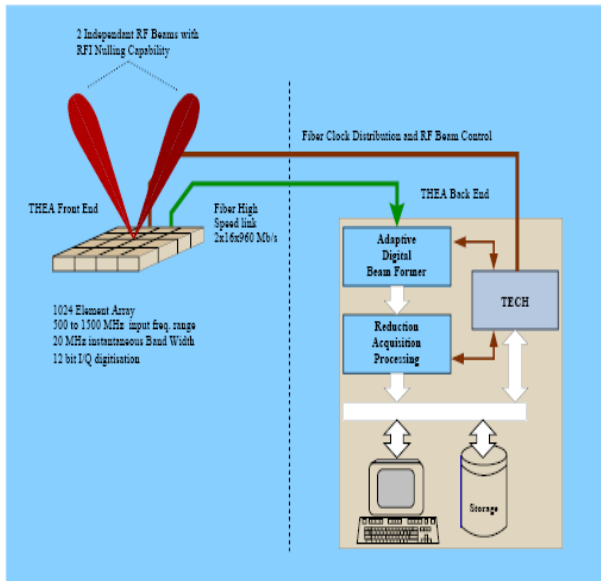


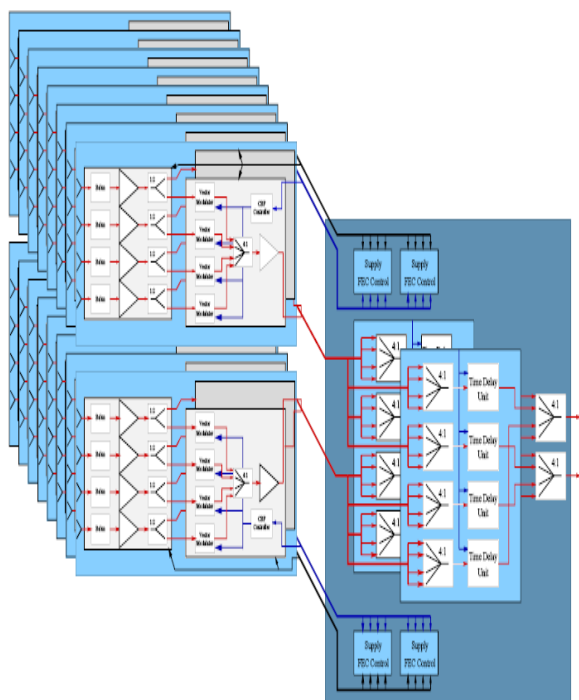
Fig.1 THEA system lay-out, consisting of 16 tiles. Each tile consists of 64 receiving antenna elements. THEA produces 32 beams simultaneously without loss of sensitivity

THEA will be an out-door phased array system that will be used to detect radio sources in the frequency band from 600 to 1700 MHz. In this paper the RF column beamformer boards that are developed for the THEA system are presented. Each board consists of four channels. The main features of the RF beamformer boards are that 1) the four broadband antenna elements are integrated with the RF electronics on a single board; 2) Each board produces two independent beams; 3) Expensive and lossy connectors and/or cables are avoided. Details of the antenna design will be discussed. In addition, the prototype layout of the RF column beamformer board will be presented with some preliminary results of the functional behaviour of the RF column beamformer boards.

2 THEA system and RF beamforming architecture

THEA is an out-door planar phased-array receive-only antenna operating in the frequency range of approx. 600 to 1700 MHz, with a degraded performance above 1500 MHz. The system consists of 1024 receiving antenna elements distributed on a regular grid over a surface of approximately 16 m². Electronic beamsteering is done with a mixed RF and digital beamforming architecture. Multiple beams over the

entire sky can be made simultaneously without loss of sensitivity. In addition, the architecture allows us to apply several RFI rejection concepts (e.g. RF deterministic nulling and adaptive digital nulling). Figure 1 shows the basic functional layout of the proposed THEA system. It consists of 16 tiles each with $8 \times 8 = 64$ receiving elements. The total number of antenna elements is 1024. The tiles form the building blocks of the THEA system. The mechanical construction allows to change the distance between the tiles. In this way, a sparse (random) array or a linear array of 16 tiles could be made. In addition, THEA could be set-up as a two-antenna interferometer. The received signals of the 64 elements in each tile are coherently combined by a RF Beamforming unit and down-converted to a digital signal with a signal bandwidth of 20 MHz. The 32 digital output signals of the tiles are distributed to a central digital adaptive beamforming unit via 32 high-speed optical links, with a total capacity of 30.72 Gbit/sec. Each tile will have two separate RF beamforming units. In this way, two independent RF beams can be made simultaneously with each tile. Within each RF-beam 16 digital beams can be made with the digital beamforming unit. In this way THEA produces 32 beams simultaneously without a loss of sensitivity. An on-line calibration facility will be available to monitor and correct the performance of each receiving element. The RF/IF and digital beamforming architecture should be designed in such a way that it maximizes the RF/IF suppression, while other essential system requirements like noise figure and dynamic range are also fulfilled. The complete RF/IF beam forming architecture can be divided into three main sections, i.e. the RF beamformer, the IF section and the IF-to-Digital Converter (IDC) section.



beamformers are implemented as multilayer boards with on one side the RF and digital control electronics for RF beam I and on the other side the electronics for RF beam II. The active components on the Column beamformer are denoted by LNA (Low Noise Amplifier), VMOD (Vector MODulator), AMP (Amplifier). The VMOD integrates the phase-shift and amplitude weighting functionality into a single device. Additional components in the Column beamformer are the balun that interfaces with the antenna, a 1 : 2 power splitter needed to make two RF beams and a 4 : 1 power combiner. Furthermore, some control electronics will be located on the board for the control of the VMOD and to be able to switch off the power supply of the LNA devices. The Column beamformer and Row beamformer are controlled by the THEA Front End Controller (TFEC). The best results are achieved with utilization of circular array with inter-element spacing of a half wavelength. The antenna gain is stable in the whole azimuth range and the levels of side lobes are lowest. By reason of circular antenna array symmetry the radiation to any direction is possibly achieved. For illustration, the antenna radiation pattern for in-phase constant feeding is shown in figure 4a and the antenna radiation pattern optimized for 210° .

The linear, rectangular and circular antenna arrays are considered and the shape of their radiation pattern and antenna radiating parameters for concrete directions were investigated. The radiation patterns are optimized for given directions with only the real positive values of magnitude at each element feeding point. The antenna configuration which can radiate to all azimuths was found. The circular antenna array with an inter-element spacing of a half wavelength has a stable gain to all the directions and the best F/S ratio from all the considered antenna arrays.

Fig.2 Global RF beamformer architecture in each tile. The RF beamformer consists of 16 Column RF beamformer modules (on the left side) and 8 Row beamformer modules (on right side). The Column RF beamformers are implemented as multilayer boards with on one side the electronics for RF beam I and on the other side the electronics for RF beam II. The Column RF beamformer consists of four antenna elements, a balun section that interfaces with the antennas, Low Noise Amplifier (LNA), 1:2 power splitter, Vector MODulator (VMOD), 4:1 power combiner, Amplifier (AMP) and some additional control electronics.

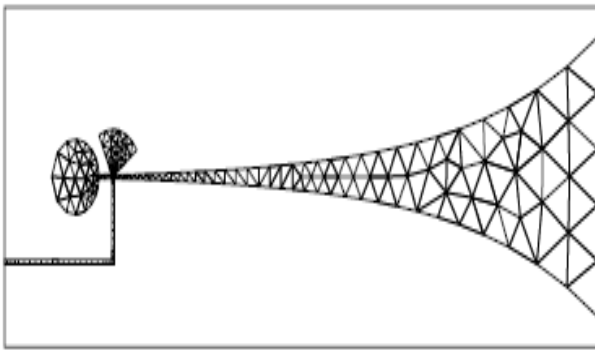
Figure 2 shows the proposed RF beamforming architecture of THEA for each tile with 64 antenna elements. The RF beamformer consists of 16 Column beamformer modules (on the left side), eight Row beamformer modules (on right side) and two passive 4:1 combiners. In the Column beamformer the signals from four antenna elements in a column are weighted in amplitude and phase and coherently combined for two RF beams. The eight output signals from the four Column beamformers in each quadrant of a tile are then input for two Row beamformer units (each for one RF beam). A Time-Delay Unit (TDU) is used in each Row beamformer to set the proper time-delays of the corresponding quadrant. Finally, the output signals from the four quadrants are combined for both RF beams in the Combiner units. The Column

3 Wideband antenna design

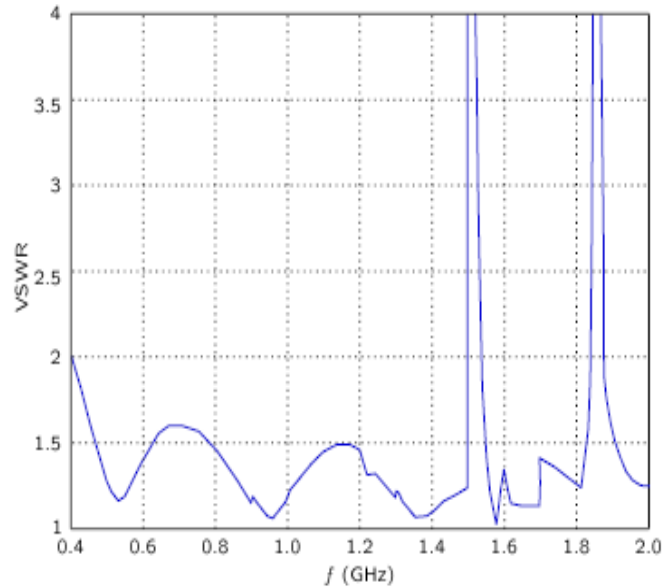
Vivaldi notch antennas have been selected for the receiving elements of the array. These elements can be used in single- or dual-polarized arrays to achieve multi octave bandwidths for scanning to 50 degrees in all planes. Full-wave method of moments analyses for infinite arrays of Vivaldi notch antennas have been developed and validated in many ways. These analyses can now be used for parameter studies [4], [5] that aid in the design of single- and dual-polarized arrays. Elements have been designed for single- and dual-scanning to 50 degrees in all planes. The results of many simulations indicate that the scan performance in the E-plane of the elements is relatively well behaved for good designs. That is, an element that is well matched in the array environment over a wide

bandwidth for broadside beam angle is usually well matched for other scan angles in the E-plane up to 40 or 50 degrees. On the other hand, the operating bandwidth for scanning in the H-plane is usually not as good as broadside and is limited at the upper end of the frequency band by anomalies that cause very high SWR over narrow bands of frequency. The lowest operating frequency of stripline-fed elements is limited in all planes by a rapid decrease in the radiation resistance of the elements. The arrays that have been designed operate without grating lobes throughout their entire frequency band and scan range. Thus, the element spacing is less than 0.5 wavelength at the highest frequency, and less than 0.1 wavelength at the lowest frequency.

Efficient operation of elements with such a small aperture relies heavily on mutual coupling to neighboring elements. Effective design of Vivaldi notch antenna arrays, therefore, requires careful treatment of mutual coupling.



(a) Vivaldi notch element for THEA



(b) Predicted SWR in infinite array

Fig.3 (a) Vivaldi notch element for THEA. Overall length = 31.5 cm; overall width = 11.25 cm. Notch aperture is 9.25 cm wide. Triangles indicate grid for MOM analysis. (b) Predicted SWR of THEA element in infinite array radiating broadside. Optimized band is 0.5 - 1.5 GHz.

The final THEA array will be comprised of Vivaldi notch elements like the one depicted in Figure 3a. The exponentially flared slotline is etched in both ground planes of the stripline circuit board that comprises the feed line. An open-circuited stripline stub at the transition provides beneficial reactance that enhances the bandwidth of the element. The circular slotline cavity terminates the slotline, but its impact on the elements radiation cannot be ignored. The full-wave MOM analyses correctly account for these effects as well as other mutual coupling effects in the array. The element will be fabricated on a dielectric substrate of thickness 0.32 cm and $\epsilon_r = 3.38$. The elements are arranged in a single-polarized, square lattice spaced 11.25 cm between centers. This spacing permits grating lobes to enter visible space at about 1.5 GHz for the maximum scan angle. The element performance would improve if the spacing were reduced, but THEA will use this spacing in order to achieve maximum array size for a fixed number of elements. In an infinite array, the element SWR is predicted in Figure 3b. The expected performance over the optimized band of 0.5 - 1.5 GHz is similar for θ up to 45 degree in the E-plane. For H-plane scanning, the elements display several

resonances. Vias will be required to suppress these resonances [6].

4 Dual beam four channel RF beamformer broad with integrated antenna elements.

The functional layout of the column RF beamformers boards was already shown in Figure 2. The column RF beamformer is implemented as a multi-layer board with a total of eight layers. The substrate material is RO 4003 with $\epsilon_r = 3.38$. The total thickness of the prototype board is 1.8 mm. The layout of the prototype beamformer board is shown in figure 4. The prototype board contains bow-tie elements.

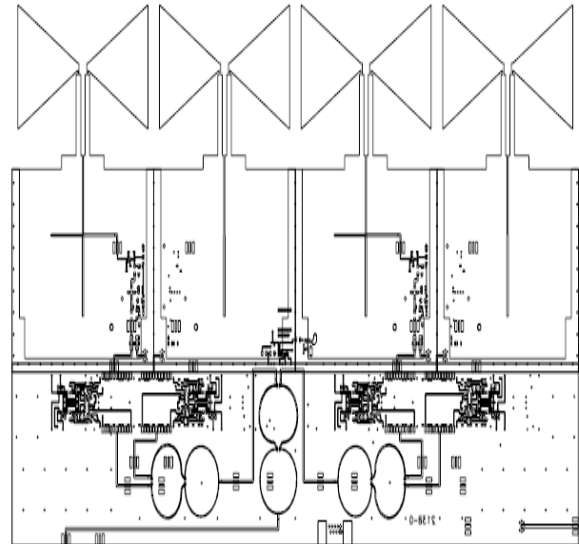


Fig. 4. Physical lay-out file of the beamformer board with integrated antenna elements.

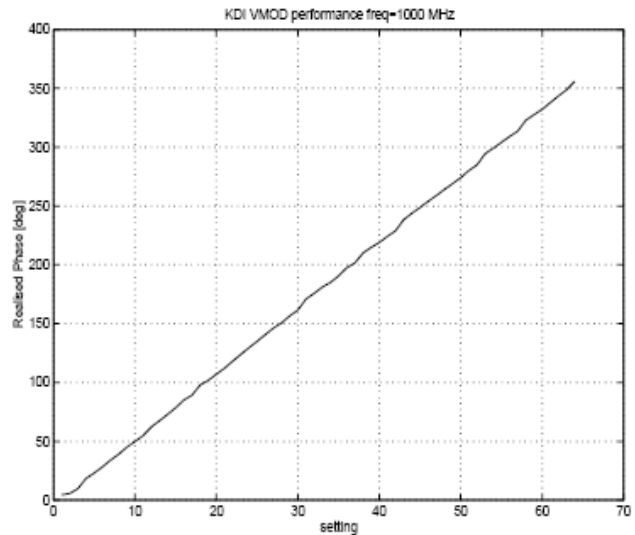
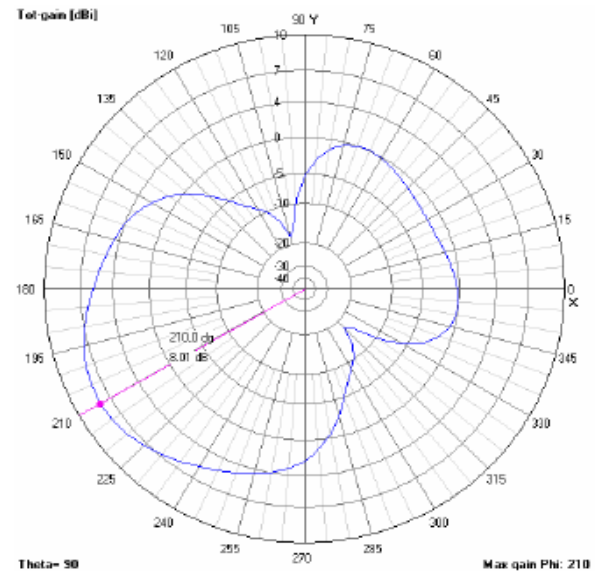


Fig.5 Measured phase versus setting of a single channel of the column beamformer, $f = 1$ GHz. The S phase error w.r.t. the ideal phase is 1.2 degree.

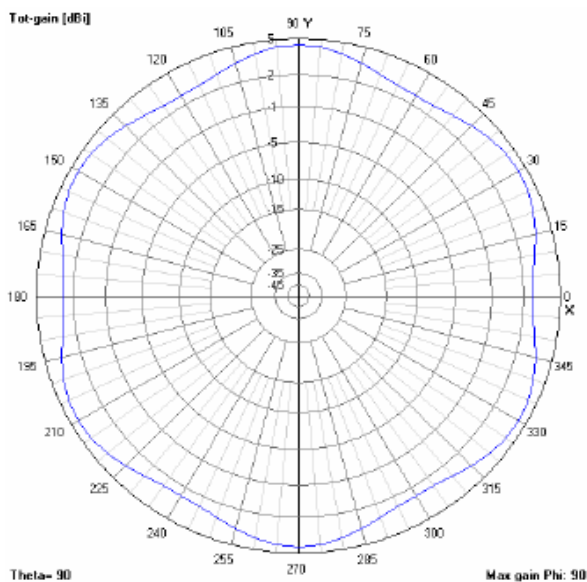
The best results are achieved with utilization of circular array with inter-element spacing of a half wavelength. The antenna gain is stable in the whole azimuth range and the levels of side lobes are lowest. By reason of circular antenna array symmetry the radiation to any direction is possibly achieved.

o



b)

Fig.6 Circular array radiation pattern a) in phase constant feeding b) optimized 210



a)

The best results are achieved with utilization of circular array with inter-element spacing of a half wavelength. The antenna gain is stable in the whole azimuth range and the levels of side lobes are lowest. By reason of circular antenna array symmetry the radiation to any direction is possibly achieved[8]. For illustration, the antenna radiation pattern for in-phase constant feeding is shown in figure 4a and the antenna radiation pattern optimized for 210° is shown in figure 6b.

Fig 7 shows beamforming network with central signal processors[9].

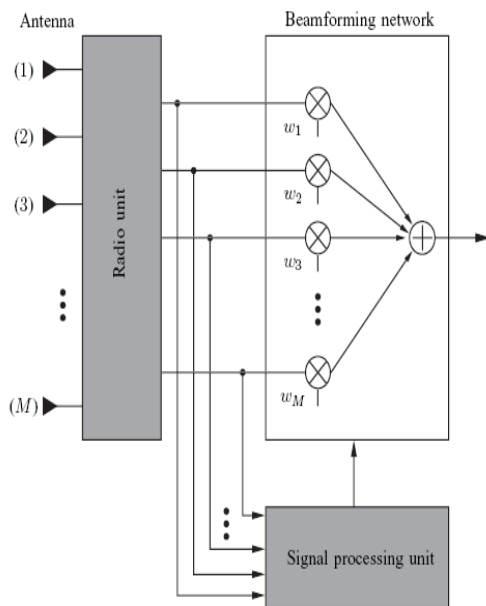


Fig.7 beamforming network

5 Antenna testing

Most of the antenna measurements were performed at the 'Compensated Compact Range' (CCR) test facility. The CCR is based on the principle that a spherical wave coming from a source antenna is converted into a plane wave by means of two focusing, precision reflectors, arranged in optimized geometry in a closed anechoic chamber.

Due to the concept of two compensated doubly curved reflectors, no test system introduced cross-polarization occurs in the test zone for both linear and circular polarization. Excellent amplitude and phase uniformity[10].

in the test zone is obtained by the large equivalent focal length of 37 m of the two-reflector system.

The complete test chamber is covered with pyramidal absorbers with a 10 to 30 cm height. The absorber layout is determined by the operation frequency range of 2.0 to 200 GHz and the main course of the rays.

During the measurements the DUT (Device under Test) is mounted on a positioner, which allows a three axes movement (azimuth, polarization and one linear axis). Especially for the determination of the phase centre of the DUT, the linear axis movement is applied.

For further improvement of the measurement accuracy, a 'hardgating' system is available [5]. This device suppresses interfering signals while maintaining the real-time test capability. The CCR test facility was used during the current design activities for the measurement of the gain and phase pattern of the Ku-band and S-band prototype antennas for the Flight Segment.

6 Measurement Results

configurations of the Ku-band antenna to investigate in particular the influence of chokerings (Fig 8) and different mounting position on top of the ACES payload. For each configuration gain and phase diagrams were recorded within an azimuth range of -120 to +120 degree and for different polarization angles.



Fig.8 Ku band antenna with 4 chocherings.

In Fig. 9 some typical results from relative gain measurements at 14.7 GHz for the antenna configuration with four chokerings (Fig. 8) are shown. The corresponding phase diagrams are depicted in Fig. 10.

plotted in Fig. 11 and Fig. 12 for the full elevation range and over time respectively[11]. The resulting signal dynamic range of about 14 dB is fully compliant with the requirements.

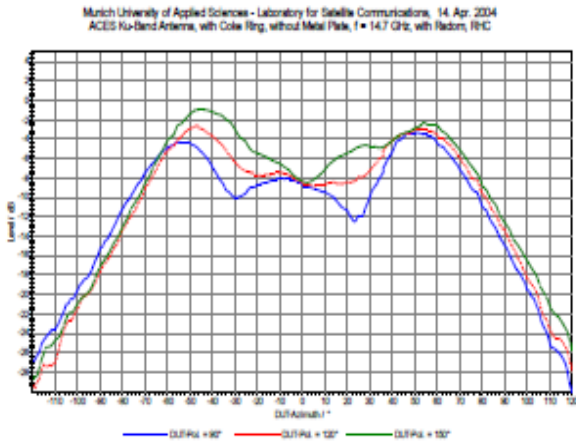


Fig.9 measured gain pattern in Ku band

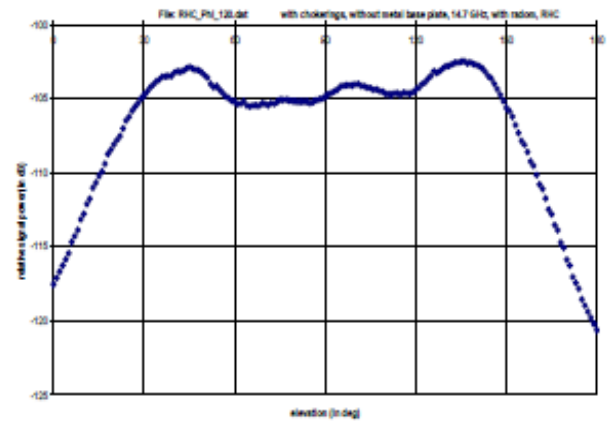


Fig. 11 Receiver Input Signal Power wrt Elevation

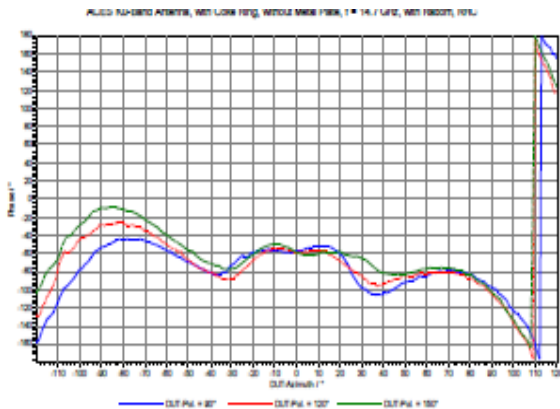


Fig.10 measured phase pattern in Ku band

From the measured gain pattern the expected variations of the signal power at the Ku-band receiver input were calculated taking into account the orbital behaviour of the ISS. For a pass through zenith, typical results are

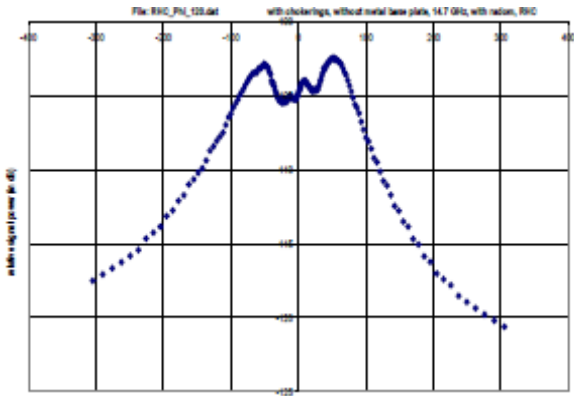


Fig.12 Receiver Input Signal Power wrt Time

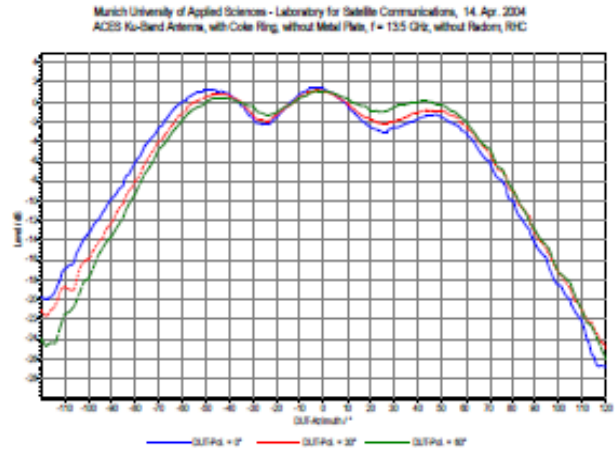


Fig.13 Gain Pattern without Metal Plate

Similar measurements were also performed with an antenna configuration with a flat ground plane instead of the chokering. In direct comparison the chokering design shows a better decrease of gain beyond 70 degree with positive impact on multipath suppression. For investigation of the influence of the ACES base plate, the chokering antenna was mounted on top of a metal plate (510mm x 510 mm). The distance between antenna and metal plate was changed between 0 mm and 75 mm. Fig. 13 and Fig. 14 are showing exemplary measurement results at 13.5 GHz with and without metal plate. With metal plate the diagram shows characteristic ripples which are resulting from interferences of the direct wave with signals reflected from the metal plate. By varying the distance between antenna and plate the ripple pattern changes accordingly. By reducing the distance the number of ripples decreases and their amplitudes increases.

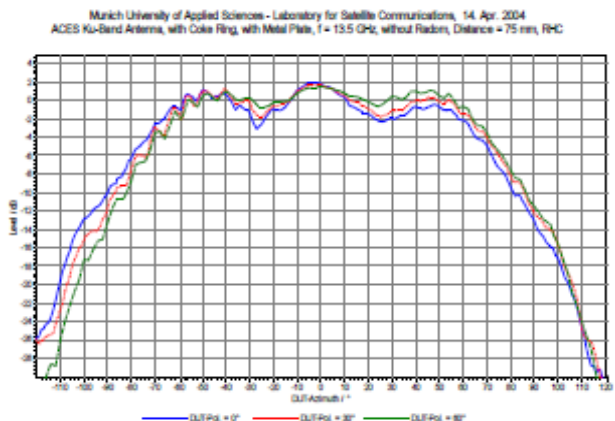


Fig.14 Gain Pattern with Metal Plate

An additional test session was performed to investigate the influence of MLI (Multi Layer Insulation) on top of the ACES surface. For the test the MLI was bulged partly for some millimeter. The effect on the phase diagram is depicted in Fig. 17. The recorded phase changes which are up to 4 degree are not acceptable with respect to the required phase center stability. As a

consequence another kind of thermal insulation will be used for the ACES payload.

The S-band antenna was tested with several ground plane configurations (outer diameters 262 mm) with and without chokerings in order to investigate their influence on the radiation pattern. No significant improvement of the gain characteristic with chokerings could be found. On the other hand the chokering design implies a significant increase in mass[12]. For that reason the baseline design for the S-band antenna will be a turnstile feed on a flat metallic ground plane. Fig. 15 and Fig. 16 are showing typical measurement results for gain and phase pattern.

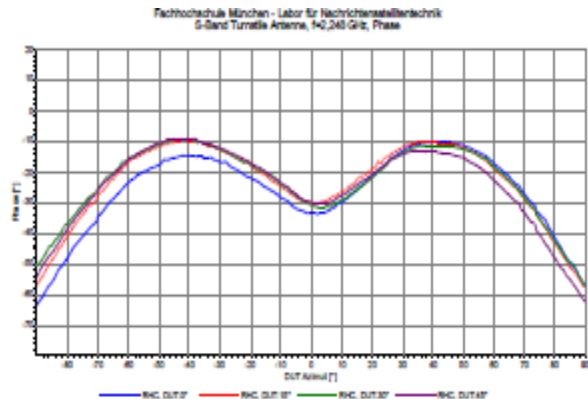


Fig.16 Measured Phase Pattern for S-band

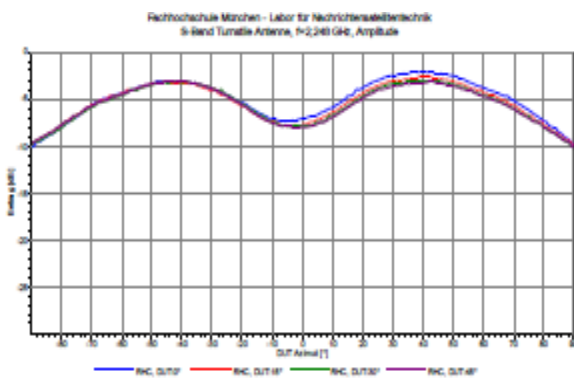


Fig.15 Measured Gain Pattern for S-band

7 Conclusion

The general approach to building a prototype for the next generation of radio telescopes, the Square Kilometer Array (SKA), was given. The prototype is a 1024-element receive-only phased-array antenna, called the Thousand Element Array (THEA). The design of a four-channel dual-beam RF beamformer board was presented. The board consists of a multilayer structure on which the four antenna elements, RF electronics and additional digital control electronics are integrated. Measured results of the functional behaviour obtained with a prototype board were presented. The linear, rectangular and circular antenna arrays are considered and the shape of their radiation pattern and antenna radiating parameters for concrete directions were investigated. The radiation patterns are optimized for given directions with only the real positive values of magnitude at each element feeding point. The antenna configuration which can radiate to all azimuths was found. The circular antenna array with an inter-element spacing of a half wavelength has a stable gain to all the directions and the best F/S ratio from all the considered antenna arrays.

References:

- [1] A. van Ardenne and F. M. A. Smits, “*Technical Aspects for the Square Kilometer Array Interferometer*,” ESTEC Workshop on Large Antennas in Radio Astronomy, The Netherlands, WPP-110, 1996, 117–127.
- [2] R. Braun, “*The Square Kilometer Array Interferometer*,” The Westerbork Observatory, Continuing Adventure in Radio Astronomy, 1996, pp. 67–184 Edited by E. Raimond and R.O. Genee, Kluwer, Dordrecht.
- [3] A. B. Smolders and G. A. Hampson, “*Deterministic RF Nulling in Phased Arrays for the Next Generation of Radio Telescopes*,” 1999 Submitted to the IEEE Transactions on Antennas and Propagation.
- [4] J. Shin and D. H. Schaubert, “*A parameter study of stripline-fed Vivaldi notch-antenna arrays*,” IEEE Transactions on Antennas and Propagation, AP-47199, pp. 879-886.
- [5] T-H. Chio and D. H. Schaubert, “*Parameter study and design of wideband, widescan dual-polarized tapered slot antenna arrays*,” accepted for publication in IEEE Transactions on Antennas and Propagation.
- [6] H. Holter, T-H. Chio and D. H. Schaubert, “*Elimination of impedance anomalies in single- and dual-polarized endfire tapered slot phased arrays*,” January 2000, to appear IEEE Transactions on Antennas and Propagation.
- [7] KAMIYA, Y., KARASAWA, Y., DENNO, S., MIZUGUCHI, Y. *A software antenna: Reconfigurable adaptive arrays based on eigenvalue decomposition*. IEICE Trans. On Communication, E82-B, vol 12, 1999.
- [8] Bellofiore, S., Balanis, C. A., Foutz, J., and Spanias, A. S.: *Smart Antenna Systems for Proceedings of the EFTF Congress 2004*, Poster Session.
- [9] *Microwave Link for ACES, Phase A Study, Final Report*, 1999, ESTEC Contract 13671/99/NL/JS.
- [10] Fockersperger S., Bedrich S., Schafer W., *Design Status of the ACES Microwave Link*, Proceedings of the EFTF Congress, 2004, Poster Session.
- [11] Hartmann J., Fasold D., *Identification and Suppression of Measurement Errors in Compact Ranges by Application of an Improved Hardgating System*, Proceedings of 22nd ESTEC Antenna Workshop, 1999.
- [12] *ACES MWL Field-of-View and Multipath Analysis*, 2003, Project Technical Note.